Oncogene
https://doi.org/10.1038/s41388-018-0522-7

ARTICLE

# Quantitative proteomics analysis identifies MUC1 as an effect sensor of EGFR inhibition

H. Rudolf de Boer[1] · Martin Pool[1] · Esméé Joosten[1] · Marieke Everts[1] · Douwe F. Samplonius[2] · Wijnand Helfrich[2] · Harry J. M. Groen[3] · Suzanne van Cooten[1] · Fabrizia Fusetti[4] · Rudolf S. N. Fehrmann[1] · Elisabeth G. E. de Vries[1] · Marcel A. T. M. van Vugt[1]

Received: 23 February 2018 / Revised: 30 July 2018 / Accepted: 6 September 2018


## Abstract

Tumor responses to cancer therapeutics are generally monitored every 2–3 months based on changes in tumor size. Dynamic biomarkers that reflect effective engagement of targeted therapeutics to the targeted pathway, so-called "effect sensors", would fulfill a need for non-invasive, drug-specific indicators of early treatment effect. Using a proteomics approach to identify effect sensors, we demonstrated MUC1 upregulation in response to epidermal growth factor receptor (EGFR)-targeting treatments in breast and lung cancer models. To achieve this, using semi-quantitative mass spectrometry, we found MUC1 to be significantly and durably upregulated in response to erlotinib, an EGFR-targeting treatment. MUC1 upregulation was regulated transcriptionally, involving PI3K-signaling and STAT3. We validated these results in erlotinib-sensitive human breast and non-small lung cancer cell lines. Importantly, erlotinib treatment of mice bearing SUM149 xenografts resulted in increased MUC1 shedding into plasma. Analysis of MUC1 using serial blood sampling may therefore be a new, relatively non-invasive tool to monitor early and drug-specific effects of EGFR-targeting therapeutics.

## Introduction

Tumor response to cancer treatment is currently assessed according to RECIST 1.1 criteria, which involve measuring changes in tumor size every 2–3 months[1]. This response may take several weeks to months to become apparent and therefore does not allow for an early assessment of efficacy of anticancer agents. Assessing the efficacy of individual anticancer therapeutics is further challenged by the fact that they are frequently used in combination therapies. Especially in early phase trials with combination therapies, there are often challenges to determine the optimal timing, duration and efficacy of novel drug treatment[2]. Providing more frequent and more drug-specific insights into drug efficacy may therefore improve assessment of tumor responses to guide clinical decision making, refine study designs, and reduce unnecessary drug exposure. In particular, a drug-specific indicator for tumor effects that can be measured non-invasively and repeatedly would enable the assessment of individual drug contribution, thus providing an effect sensor[3,4].

Ideally, effect sensors are dynamic markers that can either be detected on tumor cells or are released by tumor cells as circulating biomarkers. Multiple complementary methods have been used to non-invasively assess dynamic biomarkers, including circulating biomarkers and molecular imaging of tumor biomarkers[5]. Circulating biomarkers allow fast and high-frequency sampling due to ease of

**Electronic supplementary material** The online version of this article (https://doi.org/10.1038/s41388-018-0522-7) contains supplementary material, which is available to authorized users.

✉ Marcel A. T. M. van Vugt
m.vugt@umcg.nl

[1] Department of Medical Oncology, University Medical Center Groningen, University of Groningen, Hanzeplein 1, 9713GZ Groningen, Netherlands

[2] Department of Surgical Oncology, University Medical Center Groningen, University of Groningen, Hanzeplein 1, 9713GZ Groningen, Netherlands

[3] Department of Pulmonary Diseases, University Medical Center Groningen, University of Groningen, Hanzeplein 1, 9713GZ Groningen, Netherlands

[4] Department of Biochemistry, Groningen Biomolecular Sciences and Biotechnology Institute, Netherlands Proteomics Centre & Zernike Institute for Advanced Materials, University of Groningen, Groningen, Netherlands

Published online: 10 October 2018

collection. Circulating biomarkers have indicated early response, such as response measured with the surrogate response marker prostate-specific antigen in prostate cancer[6]. Likewise, developing tumor heterogeneity could be measured based on circulating tumor DNA[7]. Tumor biomarkers can also be visualized by molecular imaging, which has the ability to measure inter-lesion heterogeneity[8]. However, biomarkers that dynamically measure the successful targeting of tumor cells by molecularly targeted agents, which we refer to as effect sensors, are currently not available.

Here, we focused on discovery and validation of effect sensors for targeted therapies of the epidermal growth factor receptor (EGFR), an oncogenic driver in multiple cancer types that can be hyperactivated through overexpression or somatic mutation[9]. Therapeutic agents targeting EGFR, such as tyrosine kinase inhibitor erlotinib or monoclonal antibody cetuximab, provide clinical benefit in selected patient groups[10,11]. Proteome-wide analysis is highly suited for discovery of drug-specific effects in protein expression, which could be used as a generic tool to identify effect sensors[4,12]. Using mass spectrometry-based proteomics (MS proteomics), we detected early protein dynamics in response to the EGFR inhibitor erlotinib in human breast and lung cancer tumor models. We identified MUC1 as an effect sensor to monitor the effects of EGFR targeting that can be non-invasively monitored in vivo by serial blood sampling.

## Results

### Quantitative proteomic analysis of breast cancer cells identifies MUC1 in response to EGFR inhibition

To identify proteins that could be potential effect sensors of EGFR inhibition, we tested a panel of five human breast cancer cell lines expressing wt-*EGFR* for cell viability in the presence of the EGFR inhibitor erlotinib (Table 1). Three cell lines were sensitive to 10 µM erlotinib (SKBR3, SUM149, and BT474), whereas two cell lines (MB-MDA-231 and BT549) were insensitive, which was in agreement with previous reports[13,14] (Fig. 1a). Erlotinib treatment of sensitive breast cancer cells resulted in stalled proliferation as judged by the decreased cell fractions in the S/$G_2$ cell cycle phase, and an accumulation of cells in the $G_1$-phase (Sup Fig. 1A, B). Also, increased levels of apoptosis were observed upon EGFR inhibition, as evidenced by an increased sub-$G_1$ populations (Sup Fig. 1C). The cell cycle arrest was accompanied by elevated expression of the CDK inhibitor p27 and CDK1 and AKT signaling inactivation, in line with earlier reports (Sup Fig. 1D)[15].

**Table 1** Cell line characteristics

| **Histological marker** | **Cell lines** | | |
|---|---|---|---|
| **Breast cancer** | *SUM149* | *SKBR3* | *BT474* |
| Estrogen receptor | − | − | ++ |
| Progesterone receptor | − | − | − |
| HER2 receptor | − | +++ | +++ |
| EGFR expression | +++ | ++ | + |
| *EGFR* mutation status | wt | wt | wt |
| **Lung cancer** | ***H292*** | ***HCC827*** | |
| EGFR expression | ++ | +++ | |
| *EGFR* mutation status | wt | del E746–A750 | |

Summary of key histological characteristics and *EGFR* mutation status is listed for indicated cell line models

To further explore proteome-wide responses to EGFR treatment, the erlotinib-sensitive cell lines were metabolically labeled with either light or heavy isotope-labeled amino acids[16]. Next, we used mass spectrometric (MS) analysis to quantitatively measure protein abundance changes between heavy-labeled erlotinib-treated cells and light-labeled control-treated cells after 48 h, including reverse-label replicate measurements[16] (Fig. 1b). Membrane proteins were enriched using the Subcellular Protein Fractionation Kit from Thermo Fischer, which was used to separate cytosolic, membrane-bound, soluble and chromatin-bound nuclear proteins. Using stable isotope labeling of cell lines (SILAC)-MS we quantitatively detected 2131, 2120, and 1787 proteins across two independent experiments for cell lines SKBR3, SUM149, and BT474, respectively, with 1305 overlapping unique proteins (Fig. 1c). Of these, 621 (47.58%) were identified as membrane proteins using Gene Ontology annotations, of which 228 (36.71%) were plasma membrane proteins (Fig. 1c, Table S1). Among the differentially expressed proteins, PCNA and cyclin-dependent kinase 1 (CDK1) showed strongly decreased expression after erlotinib treatment, in agreement with $G_1$ cell cycle arrest in response to EGFR inactivation (Sup Fig. 1A)[17]. Independent component analysis (ICA) on the fold changes (FCs) of identified proteins was performed to separate proteomic data into statistically independent components of potential biological processes[18]. Six proteins were selected for further validation using the following criteria: proteins should be (i) expressed at plasma membranes as determined by Gene Ontology definition, (ii) induced at least by 1.5-fold, and (iii) have an ICA score above 2.0 in component 1 (Fig 1d, Table 2).

After 48 h of erlotinib treatment (10 µM) in the erlotinib-sensitive cell lines, reproducible upregulation of protein expression was observed for two of the six selected proteins in each cell line: Mucin-1 (MUC1) and ACSL1 (Fig. 2a). To test if transcriptional regulation underpinned the

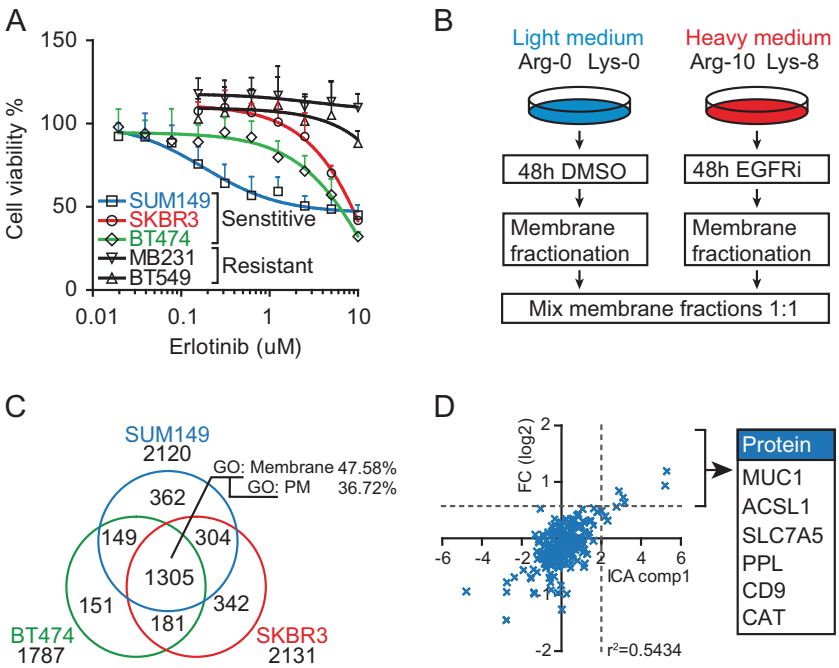


**Fig. 1** Differential protein expression by erlotinib inhibition in breast cancer cell lines. **a** Erlotinib sensitivity in breast cancer cell lines. **b** Setup of SILAC-MS. **c** Venn diagram showing the number of proteins identified per cell line, the overlap across the three cell lines, and the distribution of membrane proteins and subclassifications based on Gene Ontology analysis of the triple overlapping group. **d** Correlation between mean fold change (FC) of identified plasma membrane proteins and ICA analysis was tested by linear regression

**Table 2** Summary of proteomics results

| | Log 2 fold change | | Unique identified peptides | | |
|---|---|---|---|---|---|
| | Log2 fold | ICA score | SUM149 | SKBR3 | BT474 |
| **Upregulated** | | | | | |
| MUC1 | 1.191 | 5.304 | 3 | 2 | 3 |
| ACSL1 | 0.940 | 5.218 | 33 | 29 | 22 |
| SLC7A5 | 0.842 | 2.905 | 7 | 5 | 4 |
| PPL | 0.730 | 3.108 | 28 | 57 | 17 |
| CD9 | 0.634 | 3.165 | 7 | 7 | 5 |
| CAT | 0.560 | 2.771 | 27 | 26 | 27 |
| **Downregulated** | | | | | |
| SLC2A1 | −0.690 | −2.355 | 8 | 6 | 3 |
| ECE1 | −0.779 | −2.741 | 9 | 6 | 8 |
| RAB3D | −0.941 | −4.786 | 4 | 8 | 8 |
| RAB18 | −0.952 | −2.744 | 10 | 13 | 7 |
| CAPRIN1 | −1.448 | −2.765 | 12 | 10 | 13 |

Over- and under-expressed proteins are listed along with the numbers of unique peptides, fold changes, and results of statistical analysis using independent component analysis (ICA)

observed changes in protein expression, we analyzed mRNA expression in response to erlotinib treatment (Fig. 2b) in the six corresponding genes. Only mRNA levels of *MUC1* consistently increased in response to erlotinib treatment in the panel of erlotinib-sensitive cell lines, whereas mRNA levels were stable or showed decreased expression in erlotinib-insensitive cell lines (Fig. 2b). Notably, MUC1 protein expression was erlotinib dose-dependent, with BT474 and SUM149 cells showing increased MUC1-N and MUC1-C expression at 1.25 µM, while SKBR3 cells showed increased expression at 5 and 10 µM erlotinib (Fig. 2c). Taken together, out of a panel of six potential effect sensors for erlotinib treatment, MUC1 consistently showed erlotinib-induced upregulation, both at the mRNA and protein level in erlotinib-sensitive cell lines. MUC1 was found as top hit in our MS screens in terms of FC and ranked most significant in the first independent component of the ICA analysis (Fig. 1d). MUC1 is a plasma membrane protein consisting of an extracellular N-terminal domain (MUC1-N) and a combined transmembrane and cytoplasmic C-terminal tail (MUC1-C). MUC1 is over-expressed in many types of cancer types including breast and NSCLC[19] and can be measured in plasma of cancer patients as an indicator of tumor burden[20]. These properties make MUC1 potentially suitable as an effect sensor.

## MUC1 is upregulated by multiple EGFR-targeting strategies

As erlotinib is used in first-line treatment of NSCLC patients with activating *EGFR* mutations, we next investigated whether MUC1 upregulation also occurs in a panel of wt- or mutant-*EGFR* NSCLC cell lines (Table 1). Strong MUC1 upregulation was observed in HCC827 (*EGFR*-exon-19 deletion) and H292 (wt-*EGFR*) cell lines at 15 nM and 1 µM erlotinib, respectively (Fig. 2d), while minor MUC1 upregulation was observed in wt-*EGFR*-harboring Calu-3 and H441 cell lines at 1 and 10 µM erlotinib, respectively (Sup Fig. 2A). Similar to erlotinib-insensitive breast cancer cell lines, erlotinib-insensitive NSCLC cell

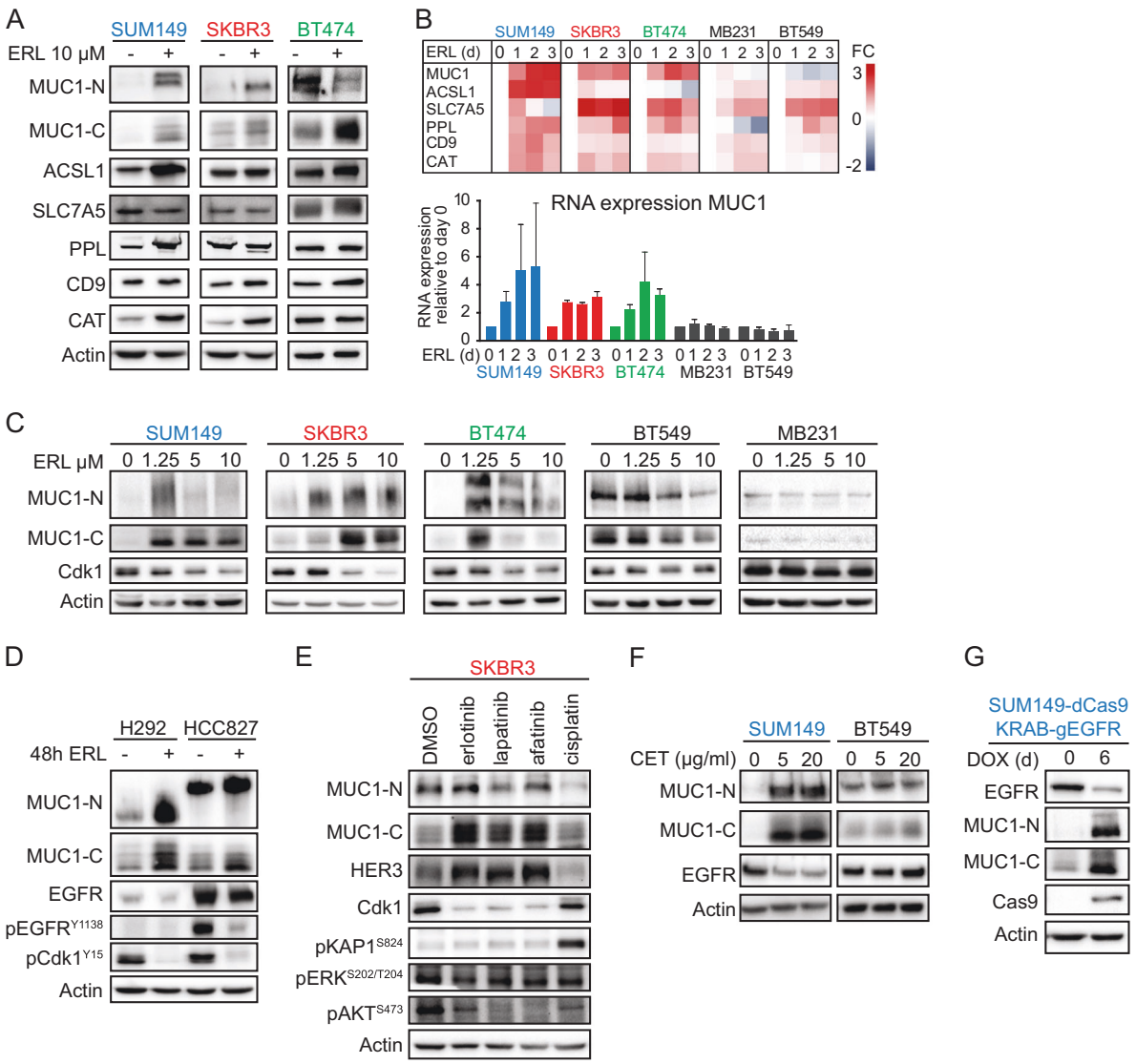


**Fig. 2** Validation of SILAC targets identifies MUC1 as effect sensor of erlotinib treatment. **a** SKBR3, SUM149, and BT474 cells were treated for 48 h with 10 µM erlotinib (ERL), and lysates were blotted for proteins selected for validation of SILAC-MS. **b** RNA expression of breast cancer cell line panel after treatment with 10 µM erlotinib for indicated periods of time. RNA expression was determined by qPCR and relative expression compared to control (0 days). Data shown of $n = 3$, and plotted as a heatmap signature, and as a bar-graph for MUC1 RNA expression. **c** Indicated breast cancer cell lines were treated for 48 h with indicated doses of erlotinib and immunoblotted for MUC1 and Cdk1 expression. **d** Lung cancer cell lines H292 and HCC827 were treated for 48 h with 1 µM and 15 nM erlotinib, respectively. **e** SKBR3 cells were treated for 48 h with DMSO, 10 µM erlotinib, 0.5 µM lapatinib, 0.05 µM afatinib, or 5 µM cisplatin. **f** SUM149 and BT549 cells were treated with 0, 5, or 20 µg/ml cetuximab for 48 h. **g** SUM149-dCas9-KRAB cells expressing a gRNA targeting EGFR were treated for 0 or 6 days with 1 µg/ml doxycycline (DOX)

lines H322 and A549 did not show MUC1 upregulation at tested doses up to 10 µM erlotinib (Sup Fig. 2A). Interestingly, a sub-clone of the HCC827 cell line (HCC827-R), which was made resistant to erlotinib through simultaneous hepatocyte growth factor treatment[21,22], no longer showed MUC1 upregulation in response to erlotinib (Sup Fig. 2B), consistent with the observed lack of MUC1 upregulation in erlotinib-insensitive breast cancer cell lines.

Besides erlotinib, other EGFR or HER-family targeting agents are in clinical use, including the tyrosine kinase inhibitors gefitinib, lapatinib, and afatinib, which target multiple HER family members, and EGFR-targeting monoclonal antibody cetuximab[23,24]. A similar increase in MUC1-C and MUC1-N was observed after 48 h treatment with gefitinib in SUM149 and SKBR3 cells (Sup Fig. 2C). Likewise, treatment of SKBR3 for 48 h with afatinib (50 nM) resulted in a clear induction of both MUC1-C and MUC1-N expression (Fig. 2e), while treatment with lapatinib (500 nM) induced MUC1, although to a lesser extent (Fig. 2e). Notably, MUC1 expression was not elevated after

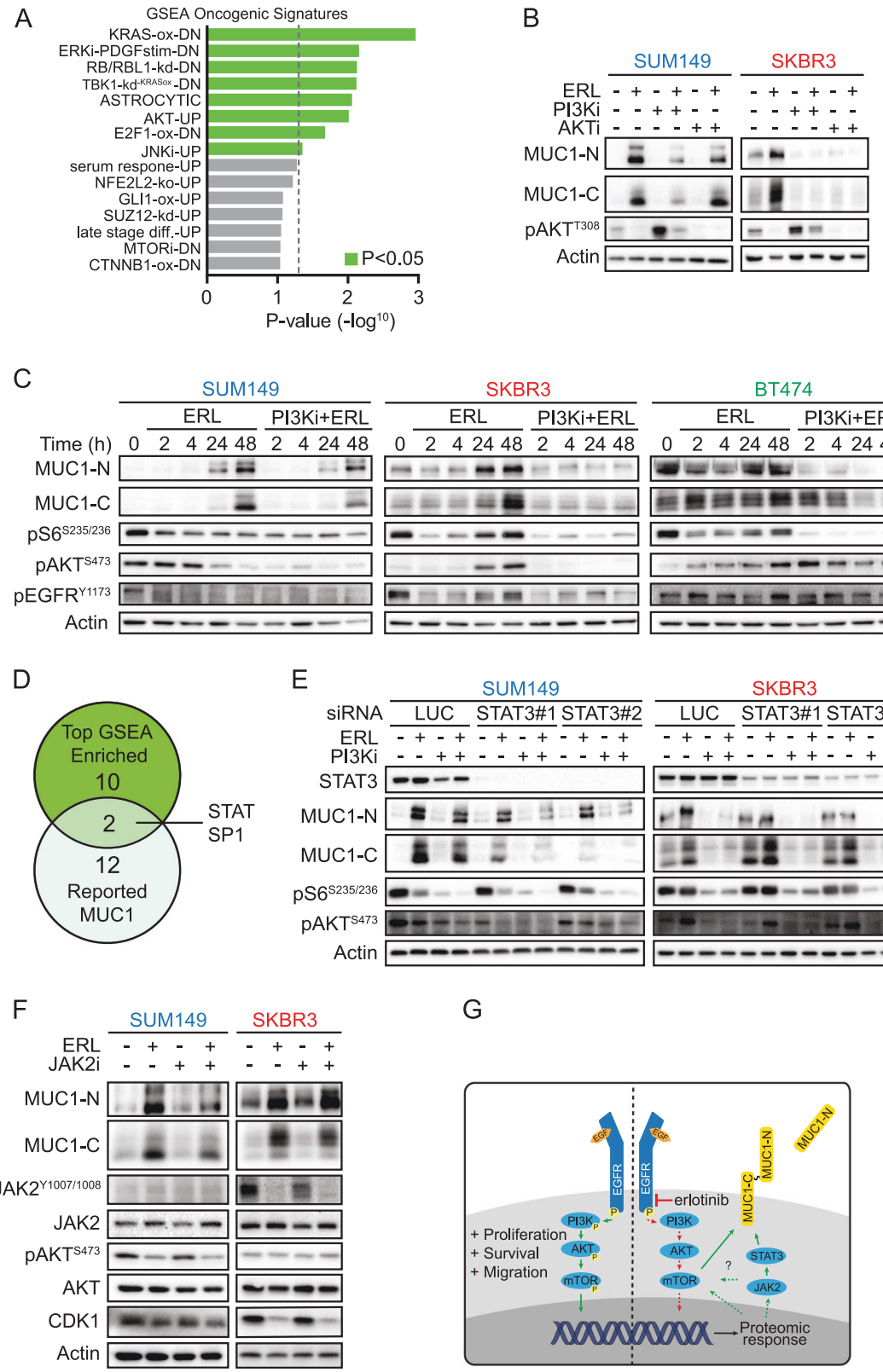


treatment with doses of the DNA-damaging agent cisplatin that robustly induced DNA damage as judged by DNA damage marker phosphorylated-KAP1 (Fig. 2e)[25]. MUC1 upregulation therefore appears to be a specific response to EGFR inactivation, rather than a generic reaction to arrested proliferation or cellular stress.

◀ **Fig. 3** MUC1 expression in response to erlotinib is dependent on PI3K/AKT/mTOR and STAT3. **a** Analysis of significantly enriched oncogenic signatures in ICA component 1. **b** SKBR3 or SUM149 cells were treated for 48 h with DMSO, PI3Ki (BEZ235), or AKTi (MK2206) alone or in combination with erlotinib (ERL; SKBR3 10 μM, SUM149 1.25 μM) and lysates were subjected to immunoblotting. **c** SUM149, SKBR3, and BT474 cells were treated with erlotinib alone or combined with PI3Ki and lysates were subjected to immunoblotting. **d** Overlap between enrichment of transcription factor profiles in ICA component 1 and in literature reported MUC1 regulating transcription factors. **e** Knockdown of STAT3 in SKBR3 or SUM149 cells for 72 h, combined with erlotinib (1.25 μM) and PI3Ki (300 nM) for 48 h. **f** SUM149 and SKBR3 cells were treated for 48 h with 1.25 and 10 μM erlotinib, respectively, alone or in combination with 5 μM JAK2 inhibitor BMS-911543. **g** Model of MUC1 induction by EGFR inhibition

We next tested whether treatment with mAb cetuximab also affects MUC1 levels. Treatment of SUM149 cells with 5 or 20 μg/ml cetuximab strongly induced MUC1 expression, which was absent in erlotinib-resistant BT549 cells (Fig. 2f). Cetuximab treatment of SKBR3 and BT474 cells, both expressing similar low EGFR levels, did not show induced-MUC1 expression (Sup Fig. 2D). As SKBR3 and BT474 cells express high levels of HER2 expression, we tested whether targeting HER2 using trastuzumab (5 or 20 μg/ml) would induce MUC1 expression. However, no changes in MUC1 expression were seen in either SKBR3 or BT474 cells, nor in low HER2-expressing SUM149 and BT549 cells (Sup Fig. 2E). This again indicates that at MUC1 expression is selectively upregulated in response to EGFR targeting in these models.

MUC1 expression was shown to attenuate apoptosis in response to genotoxic agents[26]. Thus, it is conceivable that MUC1 fulfills a similar role in protecting cells against EGFR inhibition as a potential resistance mechanism. To test this notion, SUM149 cells were transfected with a doxycycline-inducible, catalytically-inactive Cas9 (dCas9) fused to transcriptional repressor KRAB, or fused to transcriptional activator VP64, together with *MUC1* promoter targeting guide RNAs, to respectively repress or activate targeted *MUC1* gene expression[27–29]. Although MUC1 expression was successfully silenced or overexpressed in SUM149, erlotinib sensitivity was not altered in short- or long-term survival assays (Sup Fig. 3A–F). These data show that in our models MUC1 is not required for tumor cell survival upon EGFR targeting.

Thereafter CRISPRi was used to transcriptionally repress the *EGFR* promoter to validate MUC1 genetically. Upon treatment with doxycycline for 6 days, efficient silencing of EGFR was observed in SUM149-dCas9-*EGFR*, which was accompanied by elevation of MUC1 levels, comparable to MUC1 levels after erlotinib-mediated EGFR inhibition (Fig. 2a, g). Notably, EGFR repression resulted in durably elevated MUC1 levels for up to 12 days (Sup Fig. 2f). Thus, MUC1 upregulation appears to be a generic effect sensor for EGFR targeting, either in response to pharmacological or genetic inactivation of EGFR.

## Erlotinib-induced MUC1 expression requires PI3K/AKT/mTOR signaling

Rewiring of cellular signaling pathways can reverse the effects of EGFR inhibition on downstream signaling pathways[30–34]. For instance, increased interaction between the HER3 and c-MET receptors rescued growth inhibition induced by gefitinib in NSCLC cells[34], while increased catalytic HER3 activity reversed lapatinib-induced growth inhibition in breast cancer cells[30–33]. To test whether such pathway rewiring might explain MUC1 upregulation, we analyzed whether signatures of compensatory processes could be detected in our MS data sets. Pathway analysis on the SILAC-MS identified proteins in Fig. 1c using gene set enrichment analysis (GSEA) showed enrichment of genes affected by alterations in KRAS/ERK and AKT function (Fig. 3a). Inhibition of MEK (AZD6244) or ERK (FR18024), either alone or in combination with erlotinib, did not affect MUC1 expression levels in SKBR3 cells (Sup Fig. 4A). In contrast, inhibition of PI3K (BEZ235), AKT (MK2206), or mTOR (everolimus) effectively lowered MUC1 expression in SKBR3 cells, even in the absence of EGFR inhibition (Fig. 3b, Sup Fig. 4B). Interestingly, MUC1 expression was still maintained in SUM149 cells treated with EGFR and AKT inhibition and was only partially suppressed by inhibition of PI3K (Fig. 3b). To determine how the PI3K/AKT pathway is involved in inducing MUC1 expression, we analyzed downstream signaling of this pathway in SUM149 and SKBR3 cells after erlotinib treatment. Levels of phospho-AKT (Ser476) and phospho-S6 (Ser235/S236) were reduced at early time points after erlotinib treatment (Sup Fig. 4C). Surprisingly, however, between 7 and 24 h after treatment, levels of AKT and S6 phosphorylation were restored, which coincided with induction of both MUC1-C and MUC1-N expression at 24 and 48 h (Sup Fig. 4C). Combined inhibition of PI3K with erlotinib treatment prevented phosphorylation of AKT and S6 and interfered with MUC1 expression in SKBR3 and BT474 cells, and to lesser extent in SUM149 cells (Fig. 3c). These results indicate compensatory activation of AKT/MTOR underpinning MUC1 expression in erlotinib-treated SKBR3 and BT474 cells, while other compensatory processes may underlie MUC1 expression in SUM149 cells.

## JAK2/STAT3 drives MUC1 expression by tumor cells in response to EGFR inactivation

Since MUC1 was found to be regulated at the transcriptional level in response to EGFR inactivation, we decided to

identify the responsible transcriptional regulators. We used GSEA to search for transcription factors (TF) whose target genes are enriched in our proteomic dataset, and found enrichment of STAT and SP1, known regulators of MUC1 expression (Fig. 3d)[35–37]. To test involvement of these TFs, expression and localization of SP1, STAT1, and STAT3 in response to EGFR inhibition were investigated in SUM149 cells. Whereas no changes were detected in the amount of STAT1 or SP1 in nuclear fractions, an erlotinib-induced increase in nuclear STAT3 was observed (Sup Fig. 4D). Although some variation was observed between MUC1-N and MUC1-C, siRNA-mediated depletion of STAT3 in SUM149 cells resulted in reduced erlotinib-induced expression of both MUC1-N and MUC1-C, suggesting that STAT3 is indeed required to drive MUC1 expression under these circumstances (Fig. 3e, Sup Fig. 4G). However, STAT3 depletion in SKBR3 cells did not affect MUC1 expression (Fig. 3e), indicating that other transcriptional regulators of MUC1 are involved in its upregulation upon EGFR inhibition. Interestingly, PI3K inhibition of siLUC-treated SUM149 cells reduced STAT3 expression, and combined inactivation of PI3K and knockdown of STAT3 further reduced MUC1 expression in erlotinib-treated SUM149 cells (Fig. 3e, Sup Fig. 4F, G). Previously JAK2 was shown to function upstream of STAT3 to induce MUC1 expression[38]. Indeed, treatment of SUM149 cells, but not SKBR3 cells, with the JAK2 inhibitor BMS-911543 suppressed erlotinib-induced MUC1 expression, similar to STAT3 knockdown (Fig. 3f, Sup Fig. 4H). Thus, it appears that the JAK2/STAT3 pathway is involved in regulating MUC1 expression upon EGFR inhibition in SUM149 cells, possibly through interaction with the PI3K/AKT/MTOR signaling pathway.

## Erlotinib treatment induces lasting expression and shedding of MUC1

As CRISPR/Cas9-mediated silencing of EGFR in SUM149 cells resulted in durable MUC1 protein expression (Fig. 2g, Sup Fig. 2F), we tested whether long-term erlotinib would also induce durable MUC1 upregulation. Low-dose erlotinib treatment (1.25 μM) in SUM149 cells showed high MUC1 expression during 16 days of continuous erlotinib treatment, maintaining a four-fold increase in MUC1 (Fig. 4a). MUC1 expression increased gradually in SKBR3 and BT474 cells, reaching ~2-fold induction at 12 and 16 days, respectively; no MUC1 increase was measured in resistant cell lines BT549 and MDA-MB-231 (Fig. 4a). Thus, MUC1 appears to be durably upregulated in response to EGFR inhibition in vitro in erlotinib-sensitive cell lines.

In many cancers, shed MUC1 is known as cancer antigen 15-3 (CA 15-3), and it has been widely tested as a plasma biomarker reflecting tumor load[20]. We therefore postulated that erlotinib-induced shedding of MUC1 could be a suitable non-invasive indicator for effective erlotinib treatment. To test if MUC1 shedding occurs in our breast and NSCLC cell lines, we measured MUC1 shedding after erlotinib treatment. Similar to cellular MUC1 expression (Fig. 2), SUM149 and H292 cells increasingly released MUC1 into culture media after 48 h of erlotinib treatment, while shed MUC1 levels remained unaltered in the erlotinib non-responsive cell lines (Fig. 4b).

## Monitoring circulating MUC1 as an effect sensor of EGFR inhibition in vivo

To test whether MUC1 expression is similarly regulated upon erlotinib treatment in vivo, we first tested MUC1 expression in response to a range of erlotinib doses in SUM149 xenograft tumors in mice. Daily intraperitoneal erlotinib (0, 25, 50, or 100 mg/kg) for 9 days resulted in a dose-dependent decrease in tumor volume, underscoring erlotinib efficacy and confirming previous findings (Sup Fig 5A)[39]. Immunohistochemical (IHC) analysis of MUC1-N expression on excised tumors showed elevated MUC1 expression in 50 and 100 mg/kg erlotinib-treated mice (Sup Fig 5B). To test if shed MUC1 could be detected in vivo, SUM149-xenografted mice were treated daily for 9 days with vehicle ($n = 2$) or 50 mg/kg erlotinib ($n = 8$). Vehicle-treated, non-tumor-bearing mice ($n = 2$) were included to assess background circulating MUC1 levels. SUM149 tumor growth inhibition was clearly observed in erlotinib-treated mice after 9 days, and MUC1 expression in tumors increased (Sup Fig 5C–E). Importantly, erlotinib-treated mice showed higher shed MUC1 levels after 9 days of treatment compared to vehicle-treated mice, while non-tumor-bearing mice showed negligible shed MUC1 levels (Fig. 4c).

To assess whether changes in MUC1 cell surface expression can be non-invasively assessed using molecular imaging, the MUC1 targeting antibody VU4H5 was radiolabeled with the positron emission tomography (PET) isotope Zirconium-89 ($^{89}$Zr; $^{89}$Zr-αMUC1-mAb). Mice bearing SUM149 xenografts were treated for 9 days with daily 50 mg/kg erlotinib ($n = 7$) or vehicle ($n = 6$). $^{89}$Zr-αMUC1-mAb was injected at day 3, together with a non-specific targeting Indium-111($^{111}$In)-labeled IgG, to assess generic antibody organ and tumor uptake. However, $^{89}$Zr-αMUC1-mAb did not show increased specific tumor tracer uptake in erlotinib-treated mice (9.88 ± 1.98 %ID/g) compared to vehicle-treated mice bearing SUM149 xenografts (9.30 ± 2.01 %ID/g) ($P = 0.8537$) (Fig. 4e). Furthermore, MUC1-specific tumor uptake of $^{89}$Zr-αMUC1-mAb only marginally exceeded background levels of $^{111}$In-IgG uptake, suggesting too little sensitivity for MUC1 imaging in SUM149 tumors, similar to the lack of change in MUC1

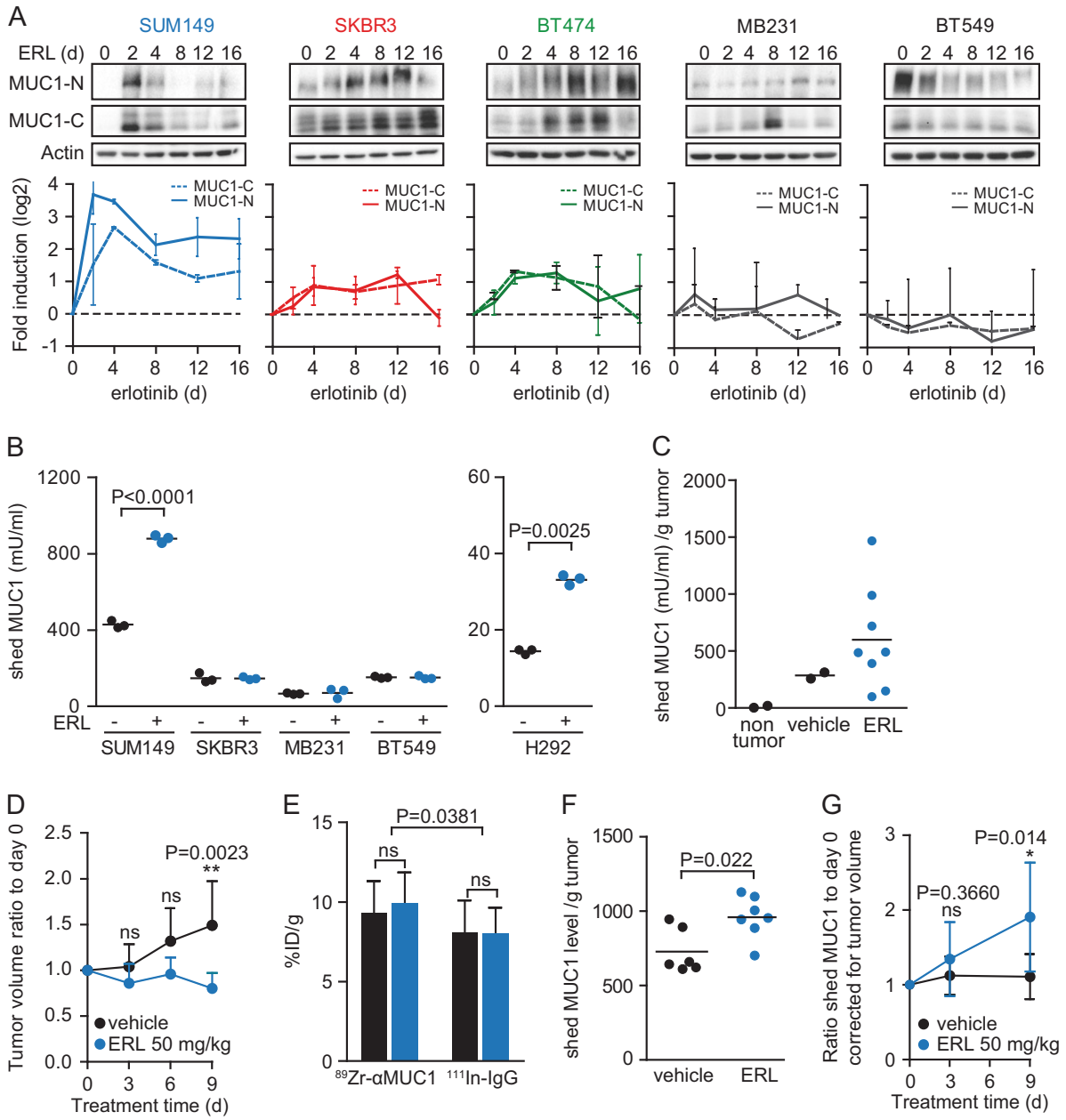


**Fig. 4** MUC1 expression and shedding upon erlotinib treatment in vitro and in vivo. **a** Breast cancer panel was treated up to 16 days with 1.25 μM erlotinib and samples were harvested at indicated time points of treatment. Lysates were immunoblotted for MUC1-C and MUC1-N, and levels were quantified and normalized to actin levels. **b** MUC1 levels in culture media of indicated cell lines after 48 h treatment with erlotinib. **c** Plasma-shed MUC1 levels per gram tumor of vehicle- or erlotinib-treated SUM149 xenograft-bearing mice. **d** Tumor volume of SUM149 xenograft tumors during 9 days of treatment with vehicle or erlotinib. **e** Activity counts of $^{89}$Zr-αMUC1-mAb and $^{111}$In-IgG accumulation tumors as percentage injected dose per gram (%ID/g). **f**, **g** Plasma levels of MUC1 were assessed at 0, 3, and 9 days after vehicle or erlotinib treatment and **f** corrected for tumor weight or **g** corrected for tumor volume

expression observed by IHC in this experiment (Fig. 4e, Sup Fig 6C–E). In parallel to molecular imaging of MUC1, we performed serial blood sampling of shed MUC1 to evaluate MUC1 expression in vivo after 0, 3, and 9 days of daily erlotinib treatment. In line with our in vitro data (Fig. 4b), serial sampling of MUC1 in plasma showed a rise in shed MUC1 visible after 3–9 days of treatment, specifically in erlotinib-treated mice (Fig. 4f, g). The observed increase in human MUC1 was not due to systemic shedding of mouse MUC1, as no significant differences could be measured in mouse MUC1 levels upon erlotinib treatment (Sup Fig 7A, B). Furthermore, we observed increased MUC1 shedding in erlotinib-treated mice, even though tumor volumes rapidly decreased due to erlotinib treatment

(Fig. 4d, f, g). This suggests that measurement of circulating MUC1 in plasma can be used to monitor early treatment response to erlotinib.

## Discussion

In this study we identified and validated MUC1 expression dynamics as an effect sensor for EGFR-targeted treatment. We observed rapid upregulation of MUC1 expression in response to EGFR-targeted treatments in human breast and lung cancer models. Treatment of a panel of breast cancer cell lines with multiple EGFR inhibitors, cetuximab, or genetic inactivation of *EGFR* invariably resulted in increased MUC1 protein expression. MUC1 upregulation was durable, both in vitro and in vivo, and shed MUC1 in plasma levels reflected treatment efficacy of erlotinib. Our results warrant further testing of MUC1 as a non-invasive effect sensor to monitor early treatment effects of EGFR inhibition.

AKT/mTOR and STAT3 were found to be involved in upregulation of MUC1 expression upon EGFR treatment in the breast cancer panel. Our data show reactivation of AKT and S6 activity after initial silencing upon erlotinib treatment (Fig. 3c). These observations are in line with multiple reports showing dynamic rewiring of the AKT pathway in response to pharmacological targeting of upstream signaling components, involving RTKs such as HER3 and IGF1R as compensatory activators[32–34]. Furthermore, JAK2–STAT3 was required for MUC1 expression in SUM149 cells and may be driven by IL-6 signaling as was reported in lung cancer and prostate epithelial cell lines[38,40]. As we found multiple pathways to be able to regulate MUC1 in response to erlotinib, further investigation is warranted to test whether this is due to cancer subtype-specific disposition towards specific signaling pathways.

Using a SILAC proteomic approach, we identified membrane proteins that become more abundant after EGFR treatment. Although this approach does not yet capture complete proteomes[41], by identifying the most abundantly expressed proteins, MUC1 was detected across three cell lines of different breast cancer subtypes. MUC1 was not detected in a previous SILAC approach using gefitinib in epidermal cell line A431, which was concordant with our results with this cell line (Sup Fig. 2A), underscoring potential differential responses between cancer subtypes[12]. Furthermore, MUC1 expression was not altered by cisplatin treatment in SKBR3 cells (Fig. 2e), further demonstrating that the induction of MUC1 expression is a specific effect of EGFR targeting. Our approach to identify effect sensors can be easily applied to other targeted therapies as well as to conventional chemotherapeutic agents, including cisplatin, to develop drug-specific readouts for monotherapies and combination therapies.

The cell line panel that we used included mostly wt-*EGFR* models, and one *EGFR* mutant model (HCC827, Table 1). Although small-molecule EGFR inhibitors are used in the clinical for *EGFR* mutant cancers, also in *EGFR*-wt tumors, activity of the EGFR can have oncogenic properties[42]. Importantly, we observed upregulated MUC1 both in wt-*EGFR* models and *EGFR* mutant models, reflecting similar cellular rewiring upon EGFR inhibition.

We tested the use of MUC1 as effect sensor in vivo as a shed biomarker in plasma and as a target for molecular imaging. Although we detected MUC1-specific $^{89}$Zr-αMUC1-mAb uptake in tumors using molecular imaging, we did not achieve sufficient contrast to detect erlotinib-induced changes in MUC1 expression when compared to generic $^{111}$In-IgG antibody distribution. Low MUC1 expression levels on SUM149 cells and shed MUC1 redirecting $^{89}$Zr-αMUC1-mAb to the liver, as evidenced by enhanced liver uptake (Sup Fig 6D, E), could have interfered with accumulation of $^{89}$Zr-αMUC1-mAb in tumors and precluded sufficient dynamic range for molecular imaging in this experimental setup[43].

Similar to in vitro measurements, increased MUC1 shedding in plasma of human tumor-bearing mice could be detected by serial sampling in response to erlotinib treatment. Our results point towards analysis of both pre-treatment levels of MUC1 as well as early follow-up measurements to monitor efficacy of EGFR-targeted therapy. Ideally, multiple longitudinal samples should be measured to also be able to assess MUC1 levels when patients relapse, which invariably occurs. Interestingly, serial sampling of MUC1 plasma levels in 70 NSCLC patients showed increasing MUC1 levels after 2 and 4 weeks of gefitinib in patients with progressive disease[44]. This time frame likely involves significant changes in tumor volume, and in this time frame MUC1 levels could reflect tumor burden of drug-resistant tumor cells, in line with high pre-treatment levels of MUC1 being prognostic for worse survival to gefitinib-treatment[45,46]. Alternatively, it could indicate that MUC1 expression is part of an adaptation mechanism of tumor cells to restore oncogenic properties. Clearly, further study is required to characterize the early dynamics of MUC1 shedding in properly selected EGFR inhibitor-treated cancer patients. Such studies should include tumor size measurements, and longitudinal blood sampling to establish whether MUC1 shedding in response to EGFR inhibition can contribute to assessment of treatment response by RECIST criteria. Our results warrant clinical assessment of shed MUC1 as an effect sensor, aiming to stratify patients for treatment with EGFR therapeutics.

## Materials and methods

Detailed description can be found in Supplemental Materials and Methods for: cell line cultures conditions; antibodies and gRNA sequences used; MS instrument settings; in vivo PET imaging

### Cell lines, SILAC labeling, and reagents

Human breast cancer cell lines SKBR3, BT474, BT549, and MDA-MB-231; human non-small cell lung cancer cell lines H292 and HCC827; and HEK-293T were obtained from American Type Culture Collection (ATCC). SUM149 cells were a gift from Prof. W.T.A. van der Graaf (Medical Oncology, Radboud University Nijmegen Medical Centre, Nijmegen, The Netherlands). Stable isotope labeling of cell lines (SILAC) was done using RPMI or DMEM-high glucose media with normal Arg and Lys (light) or $Arg^{10}$ and $Lys^{8}$ (heavy) (Silantes). Human MUC1 shedding was measured using a standardized MUC1 human ELISA kit (EHMUC1; Thermo Scientific), mouse MUC1 was measured using a MUC1 mouse ELISA kit (E-EL-M2604; Elabscience). MUC1 has a reported serum half-life of ~7 days[47]. The following inhibitors were used: EGFR inhibitors erlotinib (LC Laboratories; Axon Medchem), gefitinib (Axon Medchem), lapatinib (LC Laboratories), afatinib (Tocris); JAK2 inhibitor BMS-911543 (Selleckchem); PI3K inhibitor BEZ235, AKT inhibitor MK2206, mTORC1/2 inhibitor everolimus, ERK inhibitor FR18024, MEK1 inhibitor AZD6244 (Axon Medchem).

### Animal experiments

Male nude mice (BALB/cOlaHsd-Foxn1nu; Envigo) were subcutaneously inoculated with SUM149 xenograft tumors. Mice with tumors >200 $mm^3$ were included. Blood (100 µl) was sampled retro-orbitally under anesthesia, after which daily treatment commenced with either 50 mg/kg erlotinib in 30% Captisol or vehicle via intraperitoneal injection. Generation of $^{89}$Zr-αMUC1-mAb, ex vivo organ biodistribution analysis, microPET scans, scan reconstruction, and quantification were performed similarly as described previously[43]. All animal experiments were approved by the Institutional Animal Care and Use Committee of the University of Groningen.

### Plasmids and transfections

For dCAS9-CRISPR-mediated regulation of gene expression, pHAGE-TRE-dCAS9-KRAB (CRISPRi), pHAGE-TRE-dCAS9-VP64 (CRISPRa), and pLKO.1-puro U6 (a gift from Rene Maehr & Scot Wolfe; Addgene plasmids #50917, #50916 and #50920) were used as described previously[28]. pHAGE-TRE-dCAS9-KRAB or pHAGE-TRE-dCAS9-VP64 was transfected in HEK-293T cells using standard calcium phosphate transfection together with pAdvantage, ΔYPR and VSV-G, as described previously[48]. gRNA sequences against EGFR and MUC1 were selected from published gRNA libraries[29].

### IHC and immunoblotting

MUC-N (Cell Signaling, #4538) and MUC1-C (Thermo Scientific, #MA5-11202) were used for IHC and immunoblotting of MUC1. Membranes were visualized using a ChemiDoc in combination with Quantity One 4.5.0 software (Bio-Rad). For IHC analysis, antigen was retrieved using a 10 mM sodium citrate pH 6.0 buffer, stained for MUC1 at 1:100 dilution, and counterstained with hematoxylin staining of nuclei. MUC1-N expression by IHC was assessed using an *H*-score composed of the intensity of staining (0 = negative; 1 = weak; 2 = moderate; 3 = strong) multiplied by the percentage of stained cells.

### Fractionation, LC-MS/MS, and database searching

Cell lysates for SILAC-MS were fractionated using a "subcellular fractionation kit" (Thermo Fischer) and protein concentrations were measured with the BCA assay (Thermo Scientific). Membrane fractions were mixed in 1:1 ratio protein of erlotinib-heavy/control-light and label-swapped control-heavy/erlotinib-light, subjected to gel-electrophoresis followed by in-gel trypsin digestion. Digested peptides were analyzed using a linear ion trap-Orbitrap hybrid mass spectrometer (LTQ-Orbitrap; Thermo Scientific). The MS raw data were analyzed with MaxQuant (version 1.3.0.5) containing the integrated Andromeda search engine[49,50], and searched against the UniProt human proteome build 20132802 with a false discovery rate of 0.01. From the six SILAC-MS analyses, Log2 protein ratios were compiled in a data matrix, on which ICA was performed. GSEA was performed on ICA components for enrichment of Oncogenic Signatures and TRANSFAC data sets from MSigDB.

### Statistics

Where statistics are shown for in vitro data, we used two-sided, unpaired Student's *T*-tests for analysis of two conditions and ANOVA for multiple conditions. Correlation between mean log2 FC and ICA components was performed by Spearman's correlation. Statistical analysis on data obtained from animal experiments were performed with Mann–Whitney tests. Group sizes for $^{89}$Zr-imaging were determined based on effect sizes from previous studies.

**Acknowledgements** We thank members of the Medical Oncology Department and Cancer Research Center Groningen for helpful discussions. This work is financially supported by the European Research Council (ERC-Advanced Grant ERC-2011-293-445 to E.G.E.d.V.). E.G. E.d.V. and M.A.T.M.v.V. conceived the study. H.R.d.B., E.J., S.v.C., and M.E. designed and performed in vitro experiments. E.J. and F.F. performed MS experiments and analysis. R.S.N.F. and H.R.d.B. performed pathway analysis. M.P., D.F.S., and W.H. designed and manufactured molecular imaging tools. H.R.d.B. and M.P. performed in vivo experiments. H.R.d.B., E.G.E.d.V., and M.A.T.M.v.V. wrote the manuscript and all authors contributed to editing of the manuscript. The mass spectrometry proteomics data have been deposited to the ProteomeXchange Consortium (http://proteomecentral.proteomexchange.org) via the PRIDE partner repository [51] with the dataset identifier PXD005985.

## Compliance with ethical standards

**Conflict of interest** The authors declare that they have no conflict of interest.

## References

1. Eisenhauer EA, Therasse P, Bogaerts J, Schwartz LH, Sargent D, Ford R, et al. New response evaluation criteria in solid tumours: revised RECIST guideline (version 1.1). Eur J Cancer. 2009;45:228–47.
2. Lopez JS, Banerji U. Combine and conquer: challenges for targeted therapy combinations in early phase trials. Nat Rev Clin Oncol. 2017;14:57–66.
3. de Vries EGE, THO Munnink, van Vugt MATM, Nagengast WB. Toward molecular imaging-driven drug development in oncology. Cancer Discov. 2011;1:25–8.
4. Pool M, de Boer HR, Lub-de Hooge MN, van Vugt MATM, de Vries EGE. Harnessing integrative omics to facilitate molecular imaging of precision medicine of the human epidermal growth factor receptor family. Theranostics. 2017;7:2111–33.
5. Vargas AJ, Harris CC. Biomarker development in the precision medicine era: lung cancer as a case study. Nat Rev Cancer. 2016;16:525–37.
6. Petrylak DP, Ankerst DP, Jiang CS, Tangen CM, Hussain MHA, Lara PN, et al. Evaluation of prostate-specific antigen declines for surrogacy in patients treated on SWOG 99-16. J Natl Cancer Inst. 2006;98:516–21.
7. Forshew T, Murtaza M, Parkinson C, Gale D, Tsui DWY, Kaper F, et al. Noninvasive identification and monitoring of cancer mutations by targeted deep sequencing of plasma DNA. Sci Transl Med. 2012;4:136ra68
8. de Vries EGE, de Jong S, Gietema JA. Molecular imaging as a tool for drug development and trial design. J Clin Oncol. 2015;33:2585–7.
9. Arteaga CL, Engelman JA. ERBB receptors: from oncogene discovery to basic science to mechanism-based cancer therapeutics. Cancer Cell. 2014;25:282–303.
10. Mok TS, Wu YL, Thongprasert S, Yang CH, Chu DT, Saijo N, et al. Gefitinib or carboplatin-paclitaxel in pulmonary adenocarcinoma. N Engl J Med. 2009;361:947–57.
11. Cunningham D, Humblet Y, Siena S, Khayat D, Bleiberg H, Santoro A. et al. Cetuximab monotherapy and cetuximab plus irinotecan in irinotecan-refractory metastatic colorectal cancer. N Engl J Med. 2004;351:337–45.
12. Kani K, Faca VM, Hughes LD, Zhang W, Fang Q, Shahbaba B, et al. Quantitative proteomic profiling identifies protein correlates to EGFR kinase inhibition. Mol Cancer Ther. 2012;11:1071–81.
13. Hoadley KA, Weigman VJ, Fan C, Sawyer LR, He X, Troester MA, et al. EGFR associated expression profiles vary with breast tumor subtype. BMC Genomics. 2007;8:258
14. Yamasaki F, Zhang D, Bartholomeusz C, Sudo T, Hortobagyi GN, Kurisu K, et al. Sensitivity of breast cancer cells to erlotinib depends on cyclin-dependent kinase 2 activity. Mol Cancer Ther. 2007;6:2168–77.
15. Busse D, Doughty RS, Ramsey TT, Russell WE, Price JO, Flanagan WM, et al. Reversible G(1) arrest induced by inhibition of the epidermal growth factor receptor tyrosine kinase requires upregulation ofp27(KIP1) independent of MAPK activity. J Biol Chem. 2000;275:6987–95.
16. Ong S-E, Blagoev B, Kratchmarova I, Kristensen DB, Steen H, Pandey A, et al. Stable isotope labeling by amino acids in cell culture, SILAC, as a simple and accurate approach to expression proteomics. Mol Cell Proteomics. 2002;1:376–86.
17. Wang S-C, Nakajima Y, Yu Y-L, Xia W, Chen C-T, Yang C-C, et al. Tyrosine phosphorylation controls PCNA function through protein stability. Nat Cell Biol. 2006;8:1359–68.
18. Lee S-I, Batzoglou S. Application of independent component analysis to microarrays. Genome Biol. 2003;4:R76.
19. Kufe DW. Mucins in cancer: function, prognosis and therapy. Nat Rev Cancer. 2009;9:874–85.
20. Duffy MJ, Walsh S, McDermott EW, Crown J. Biomarkers in breast cancer: where are we and where are we going? Adv Clin Chem. 2015;71:1–23.
21. Turke AB, Zejnullahu K, Wu Y-L, Song Y, Dias-Santagata D, Lifshits E et al. Preexistence and clonal selection of MET amplification in EGFR mutant NSCLC. Cancer Cell. 2010;17:77–88.
22. Pool M, Terwisscha van Scheltinga AGT, Kol A, Giesen D, de Vries EGE, Lub-de Hooge MN et al. $8^{9Z}$r-Onartuzumab PET imaging of c-MET receptor dynamics. Eur J Nucl Med Mol Imaging. 2017;44:1328–36.
23. Geyer CE, Forster J, Lindquist D, Chan S, Romieu CG, Pienkowski T. et al. Lapatinib plus capecitabine for HER2-positive advanced breast cancer. N Engl J Med. 2006;355:2733–43.
24. Sequist LV, Yang JC, Yamamoto N, O'Byrne K, Hirsh V, Mok T. et al. LUX-LUNG 3 Phase III study of afatinib or cisplatin plus pemetrexed in patients with metastatic lung adenocarcinoma with EGFR mutations. J Clin Oncol. 2013;31:1–11.
25. White DE, Negorev D, Peng H, Ivanov AV, Maul GG, Rauscher FJ. et al. KAP1, a novel substrate for PIKK family members, colocalizes with numerous damage response factors at DNA lesions. Cancer Res. 2006;66:11594–9.
26. Ren J, Agata N, Chen D, Li Y, Yu W, Huang L. et al. Human MUC1 carcinoma-associated protein confers resistance to genotoxic anticancer agents. Cancer Cell. 2004;5:163–75.
27. Gilbert LA, Larson MH, Morsut L, Liu Z, Brar GA, Torres SE et al. CRISPR-mediated modular RNA-guided regulation of transcription in eukaryotes. Cell. 2013;154:442–51.
28. Kearns NA, Genga RMJ, Enuameh MS, Garber M, Wolfe SA, Maehr R et al. Cas9 effector-mediated regulation of transcription and differentiation in human pluripotent stem cells. Development. 2013;141:219–23.
29. Gilbert LA, Horlbeck MA, Adamson B, Villalta JE, Chen Y, Whitehead EH. et al. Genome-scale CRISPR-mediated control of gene repression and activation. Cell. 2014;159:647–61.
30. Sergina NV, Rausch M, Wang D, Blair J, Hann B, Shokat KM et al. Escape from HER-family tyrosine kinase inhibitor therapy by the kinase-inactive HER3. Nature. 2007;445:437–41.
31. Chakrabarty A, Sanchez V, Kuba MG, Rinehart C, Arteaga CL. Feedback upregulation of HER3 (ErbB3) expression and activity attenuates antitumor effect of PI3K inhibitors. Proc Natl Acad Sci USA. 2012;109:2718–23.

32. Chandarlapaty S, Sawai A, Scaltriti M, Rodrik-Outmezguine V, Grbovic-Huezo O, Serra V, et al. AKT inhibition relieves feedback suppression of receptor tyrosine kinase expression and activity. Cancer Cell. 2011;19:58–71.
33. Garrett JT, Olivares MJ, Rinehart C, Granja-Ingram ND, Sanchez V, Chakrabarty A, et al. Transcriptional and posttranslational upregulation of HER3 (ErbB3) compensates for inhibition of the HER2 tyrosine kinase. Proc Natl Acad Sci USA. 2011;108:5021–6.
34. Engelman JA, Zejnullahu K, Mitsudomi T, Song Y, Hyland C, Park JO, et al. MET amplification leads to gefitinib resistance in lung cancer by activating ERBB3 signaling. Science. 2007;316:1039–43.
35. Gaemers IC, Vos HL, Volders HH, Van der Valk SW, Hilkens J. A STAT-responsive element in the promoter of the episialin/MUC1 gene is involved in its overexpression in carcinoma cells. J Biol Chem. 2001;276:6191–9.
36. Ahmad R, Rajabi H, Kosugi M, Joshi MD, Alam M, Vasir B. et al. MUC1-C oncoprotein promotes STAT3 activation in an autoinductive regulatory loop. Sci Signal. 2011;4:ra9
37. Kovarik A, Lu PJ, Peat N, Morris J, Taylor-Papadimitriou J. Two GC boxes (Sp1 sites) are involved in regulation of the activity of the epithelium-specific MUC1 promoter. J Biol Chem. 1996;271:18140–7.
38. Starsíchová A, Lincová E, Pernicová Z, Kozubík A, Soucek K. TGF-beta1 suppresses IL-6-induced STAT3 activation through regulation of Jak2 expression in prostate epithelial cells. Cell Signal. 2010;22:1734–44.
39. Ueno NT, Zhang D. Targeting EGFR in triple negative breast cancer. J Cancer. 2011;2:324–8.
40. Lee HJ, Zhuang G, Cao Y, Du P, Kim HJ, Settleman J, et al. Drug resistance via feedback activation of stat3 in oncogene-addicted cancer cells. Cancer Cell. 2014;26:207–21.
41. Aebersold R, Mann M. Mass-spectrometric exploration of proteome structure and function. Nature. 2016;537:347–55.
42. Savage P, Blanchet-Cohen A, Revil T, Badescu D, Saleh SMI, Wang YC, et al. A targetable EGFR-dependent tumor-initiating program in breast cancer. Cell Rep. 2017;21:1140–9.
43. Pool M, Kol A, Lub-de Hooge MN, Gerdes CA, de Jong S, de Vries EGE, et al. Extracellular domain shedding influences specific tumor uptake and organ distribution of the EGFR PET tracer 89Zr-imgatuzumab. Oncotarget. 2016;7:68111–21.
44. Ishikawa N, Hattori N, Yokoyama A, Tanaka S, Nishino R, Yoshioka K, et al. Usefulness of monitoring the circulating Krebs von den Lungen-6 levels to predict the clinical outcome of patients with advanced nonsmall cell lung cancer treated with epidermal growth factor receptor tyrosine kinase inhibitors. Int J Cancer. 2008;122:2612–20.
45. Fujiwara Y, Kiura K, Toyooka S, Hotta K, Tabata M, Takigawa N, et al. Elevated serum level of sialylated glycoprotein KL-6 predicts a poor prognosis in patients with non-small cell lung cancer treated with gefitinib. Lung Cancer. 2008;59:81–7.
46. Bearz A, Talamini R, Vaccher E, Spina M, Simonelli C, Steffan A, et al. MUC-1 (CA 15-3 antigen) as a highly reliable predictor of response to EGFR inhibitors in patients with bronchioloalveolar carcinoma: an experience on 26 patients. Int J Biol Markers. 2008;22:307–11.
47. D'Alessandro R, Roselli M, Ferroni P, Mariotti S, Spila A, Aloe S, et al. Serum tissue polypeptide specific antigen (TPS): a complementary tumor marker to CA 15-3 in the management of breast cancer. Breast Cancer Res Treat. 2001;68:9–19.
48. Heijink AM, Blomen VA, Bisteau X, Degener F, Matsushita FY, Kaldis P. et al. A haploid genetic screen identifies the G 1/S regulatory machinery as a determinant of Wee1 inhibitor sensitivity. Proc Natl Acad Sci USA. 2015;112:15160–5.
49. Cox J, Mann M. MaxQuant enables high peptide identification rates, individualized p.p.b.-range mass accuracies and proteome-wide protein quantification. Nat Biotechnol. 2008;26:1367–72.
50. Cox J, Neuhauser N, Michalski A, Scheltema RA, Olsen JV, Mann M, et al. Andromeda: a peptide search engine integrated into the MaxQuant environment. J Proteome Res. 2011;10:1794–805.
51. Vizcaíno JA, Côté RG, Csordas A, Dianes JA, Fabregat A, Foster JM. et al. The proteomics identifications (PRIDE) database and associated tools: status in 2013. Nucleic Acids Res. 2013;41:D1063–9.